Remarks on anelastic spherical dynamos and their transition to a buoyancy-dominated regime

Radostin D. Simitev[a,b,c], Friedrich H. Busse[b,d], Alexander G. Kosovichev[c]

[a]*School of Mathematics and Statistics, University of Glasgow – Glasgow G12 8QW, UK, EU*
[b]*Department of Earth and Space Sciences, University of California, Los Angeles – Los Angeles, CA 90095, USA*
[c]*W.W. Hansen Experimental Physics Laboratory, Stanford University – Stanford CA 94305, USA*
[d]*Institute of Physics, University of Bayreuth – Bayreuth 95440, Germany*

Abstract

We present a set of convective dynamo simulations in rotating spherical fluid shells based on an anelastic approximation of compressible fluids. The simulations extend into a "buoyancy-dominated" regime where the buoyancy forcing is dominant while the Coriolis force is no longer balanced by pressure gradients and strong retrograde differential rotation develops as a result. Dynamos in this regime are strongly dominated by dipole components but at the same time their magnetic energies are relatively small compared to the corresponding kinetic energies of the flow. Despite being relatively weak the self-sustained magnetic fields are able to reverse the direction of differential rotation to prograde and give rise to some similarities with Solar convection.

Keywords: Rotating spherical shells, Convection, Dynamo, Anelastic approximation, Differential rotation, Solar convection zone

1. Introduction

Motivation and hypotheses. The following facts about the Solar structure and dynamics are established from observations or are well-accepted assumptions in the research community. (a) Solar convection is very vigorous and turbulent with characteristic surface velocities of the order ... [**?**]; (b) Solar rotation is nonuniform but relatively slow at an average of 27 days per revolution, e.g. []; (c) Molecular viscosity of Solar plasma is nearly negligible with a characteristic value of the order of ... [**?**]; (d) The energy of the global magnetic field of the Sun is small compared to the kinetic energy of plasma motions and differential rotation does not vary much with the Solar cycle [**?**]. This suggests that Solar convection is in a "buoyancy-dominated regime" where buoyancy forces dominate over viscous, Lorentz and Coriolis forces in the momentum balance. Thus, it is of interest to study convection and dynamo action in the buoyancy-dominated regime.

In fact, non-magnetic convection in the buoyancy- dominated regime has already attracted attention. The regime was first identified by Fokal [**?**] and Gilman [6] and more recently it was studied by Aurnou et al. [1] and Gastine et al. [5]. Bousinesq models were used in [6] and [1] and an anelastic model was used in [5]. These studies consistently found that due to vigorous mixing angular momentum is homogenized within the whole volume of the shell and this leads to strong retrograde zonal flow in the equatorial region. Retrograde differential rotation in the equatorial region is antisolar. So the question arises how can the Solar convection zone be in a buoyancy-dominated regime and at the same time sustain prograde equatorial rotation. This is the question we attempt to address in this paper. To this end, we demonstrate that demonstrate that relatively weak self-sustained field will act to reverse the retrograte differential rotation thus achieving a buoyancy-dominated regime with a solar-like zonal flow.

It is well-established [2, 10] that the main effect of self-sustained magnetic field on convection is to suppress differential rotation. Dynamo action beyond the transition from rotation-dominated regime to buoyancy-dominated regime has not been previously studied.

Buoyancy-dominated regime of convection may be relevant to Neptune and Uranus. There is evidence that the magnetic field of Uranus is non-dipolar (provide references) and that the differential rotation is retrograde at the equator. Retrograde differential rotation naturally develops in the buoyancy-dominated regime and it is of interest whether the magnetic fields that are generated resemble that of Neptune and Uranus.

Aims and plan of paper. In section 2 we introduce the mathematical model based on the anelastic approximation and briefly touch on some of the numerical implementation details. In this paper we present first results from a new anelastic code. For this reason, we include in section 3 a brief validation test against the benchmark

Email address: Radostin.Simitev@glasgow.ac.uk (Radostin D. Simitev)

solutions recently presented in [8]. In secion 4 we comment in passing on some similarities between Boussinesq and anelastic convection. Section 5 is the focus of the paper. Here we discuss the properties of dynamos in the buoyancy-dominated regime of convection. We conclude in section 6 with a summary of our main results and discussion of their implications. We also outline questions for future research.

2. Mathematical model and numerical method

2.1. Anelastic equations

We consider an electrically conducting, self-gravitating, perfect gas confined to a spherical shell. The shell rotates with a fixed angular velocity $\Omega\hat{\boldsymbol{k}}$ about the vertical axis and an entropy contrast ΔS is imposed between its inner and outer surfaces.

Assuming a gravity field proportional to $1/r^2$, a hydrostatic polytropic reference state exists of the form

$$\overline{\rho} = \rho_c \zeta^n, \quad \overline{T} = T_c \zeta, \quad \overline{P} = P_c \zeta^{n+1}, \quad \zeta = c_0 + c_1 d/r, \tag{1}$$

with parameters $c_0 = (2\zeta_o - \eta - 1)/(1-\eta)$, $c_1 = (1+\eta)(1-\zeta_o)/(1-\eta)^2$, $\zeta_o = (\eta+1)/(\eta \exp(N_\rho/n) + 1)$. The parameters ρ_c, P_c and T_c are reference values of density, pressure and temperature at the middle of the shell, and the gas polytropic index n, the density scale height N_ρ and the shell thickness ratio η are defined further below. Convection and magnetic field generation set in for sufficiently large values of the entropy contrast, ΔS, and can be described by the equations of continuity, momentum, energy and magnetic flux. In the anelastic approximation [7, 8] these equations take the form

$$\nabla \cdot \overline{\rho}\boldsymbol{u} = 0, \quad \nabla \cdot \boldsymbol{B} = 0, \tag{2a}$$

$$\partial_t \boldsymbol{u} + (\nabla \times \boldsymbol{u}) \times \boldsymbol{u} \tag{2b}$$
$$= -\nabla \Pi - \tau(\hat{\boldsymbol{k}} \times \boldsymbol{u}) + \frac{\mathrm{R}}{\mathrm{Pr}} \frac{S}{r^2} \hat{\boldsymbol{r}} + \boldsymbol{F}_\nu + \frac{1}{\overline{\rho}} (\nabla \times \boldsymbol{B}) \times \boldsymbol{B},$$

$$\partial_t S + \boldsymbol{u} \cdot \nabla S \tag{2c}$$
$$= \frac{1}{\mathrm{Pr} \overline{\rho}\,\overline{T}} \nabla \cdot \overline{\kappa \rho} \overline{T} \nabla S + \frac{c_1 \mathrm{Pr}}{\mathrm{R} \overline{T}} \left(Q_\nu + \frac{1}{\mathrm{Pm} \overline{\rho}} Q_j \right)$$

$$\partial_t \boldsymbol{B} = \nabla \times (\boldsymbol{u} \times \boldsymbol{B}) + \mathrm{Pm}^{-1} \nabla^2 \boldsymbol{B}, \tag{2d}$$

where $\boldsymbol{u}$ is the velocity, $\boldsymbol{B}$ is the magnetic flux density, S is the entropy and $\nabla\Pi$ includes all terms that can be written as gradients. The viscous force, and the viscous and Joule heating,

$$\boldsymbol{F}_\nu = \frac{\rho_c}{\overline{\rho}} \nabla \cdot \hat{\boldsymbol{S}}, \quad Q_\nu = \hat{\boldsymbol{S}} : \boldsymbol{e}, \quad Q_j = (\nabla \times \boldsymbol{B})^2, \tag{3}$$

are defined in terms of the deviatoric stress tensor

$$\hat{S}_{ij} = 2\overline{\nu\rho}(e_{ij} - e_{kk}\delta_{ij}/3), \quad e_{ij} = (\partial_i u_j + \partial_j u_i)/2,$$

where double-dots (:) denotes the Frobenius inner product. We assume that the viscosity and the entropy diffusivity vary in radius as $\overline{\nu}(r) = \nu_c \overline{\rho}^k$ and $\overline{\kappa}(r) = \kappa_c \overline{\rho}^k$ with some negative power $k \le 0$, where ν_c and κ_c are their reference values at midshell. The governing equations have been nondimensionalised using the thickness of the shell $d = r_o - r_i$ as a unit of length, d^2/ν_c as a unit of time, ΔS as a unit of entropy, $\nu_c\sqrt{\mu_0\rho_c}/d$ as a unit of magnetic induction, ρ_c as a unit of density and T_c as a unit of temperature. Here, r_i and r_o are the inner and the outer radius, λ and μ_0 are the magnetic diffusivity and permeability, respectively. The system is then characterized by eight dimensionless parameters: the radius ratio, the polytropic index of the gas, the density scale number, the radial dependence power, the Rayleigh number, the ordinary and the magnetic Prandtl numbers and the Coriolis number, defined as

$$\eta = r_i/r_o, \quad n, \quad N_\rho = \ln\left(\overline{\rho}(r_i)/\overline{\rho}(r_o)\right), \quad k,$$
$$\mathrm{R} = \frac{c_1 T_c d^2 \Delta S}{\nu_c \kappa_c}, \quad \mathrm{Pr} = \frac{\nu_c}{\kappa_c}, \quad \mathrm{Pm} = \frac{\nu_c}{\lambda}, \quad \tau = \frac{2\Omega d^2}{\nu_c}, \tag{4}$$

respectively.

Since the mass flux $\overline{\rho}\boldsymbol{u}$, and the magnetic flux density $\boldsymbol{B}$ are solenoidal vector fields, it is advantageous to employ a decomposition in poloidal and toroidal components,

$$\overline{\rho}\boldsymbol{u} = \nabla \times (\nabla \times \hat{\boldsymbol{r}} r v) + \nabla \times \hat{\boldsymbol{r}} r^2 w, \tag{5a}$$
$$\boldsymbol{B} = \nabla \times (\nabla \times \hat{\boldsymbol{r}} h) + \nabla \times \hat{\boldsymbol{r}} g, \tag{5b}$$

where $\hat{\boldsymbol{r}}$ is the radial unit vector, r is its length, v, w, h and g are the poloidal and toroidal scalars of the momentum and magnetic field, respectively. Equations (2a) are then satisfied by construction. Scalar equations for v and w are obtained, and effective pressure gradients are eliminated by taking $\hat{\boldsymbol{r}} \cdot \nabla \times \nabla \times$ and $\hat{\boldsymbol{r}} \cdot \nabla \times$ of equation (2b). Similarly, equations for h and g are obtained by taking $\hat{\boldsymbol{r}} \cdot \nabla \times$ and $\hat{\boldsymbol{r}} \cdot$ of equation (2d). The resulting poloidal-toroidal equations are somewhat lengthy and will not be listed here (or may be listed in an appendix). A minor disadvantage of this representation is that a fourth-order poloidal equation is obtained.

2.2. Boundary conditions

We explore various assumptions for the boundary conditions imposed on velocity, entropy and magnetic flux at the surface of the shell. The alternatives are listed below and the particular choice will be specified in each individual case. At a no-slip, impenetrable boundary we impose

$$v = 0, \quad \partial_r v = 0, \quad w = 0. \tag{6}$$

At a stress-free, impenetrable boundary we require

$$v = 0, \quad \partial_r^2 v - \frac{\overline{\rho}'}{\overline{\rho} r} \partial_r (r v) = 0, \quad \partial_r w - \frac{\overline{\rho}'}{\overline{\rho}} w = 0. \tag{7}$$

Values of the entropy may be fixed at the boundaries, then

$$S = 1 \text{ at } r = r_i, \qquad S = 0 \text{ at } r = r_o. \tag{8}$$

Alternatively, the entropy flux may be specified at the top,

$$\partial_r S = 0 \text{ at } r = r_o. \tag{9}$$

Boundary conditions for the magnetic field may be derived from the assumption of an electrically insulating external region. The poloidal function h is then matched to a function $h^{(e)}$, which describes an external potential field,

$$g = 0, \quad h - h^{(e)} = 0, \quad \partial_r(h - h^{(e)}) = 0. \tag{10}$$

Alternatively, a perfectly conducting external region may be assumed, requiring

$$\partial_r g = 0, \quad h = 0. \tag{11}$$

Finally, the, so-called, "pseudo-vacuum" condition offers another choice,

$$g = 0, \quad \partial_r h = 0. \tag{12}$$

2.3. Numerical method

For the numerical solution of the problem we have adapted the pseudo-spectral method described by [13]. The scalar unknowns v, w, h, g and S, are expanded in Chebychev polynomials T_p in the radial direction r, and in spherical harmonics in the angular directions (θ, φ) e.g.,

$$v = \sum_{l=1}^{N_l} \sum_{m=-l}^{l} \sum_{p=0}^{N_r} V_{lp}^m(t)\, T_p\Big(x(r)\Big)\, P_l^m(\cos\theta)\, \exp(im\varphi), \tag{13}$$

where P_l^m denotes the associated Legendre functions, $x(r) = 2(r - r_i) - 1$, and N_l and N_r are truncation parameters. A system of equations for the coefficients in these expansions is obtained by a combination of a Galerkin spectral projection of the governing equations in the angular directions and a collocation constraint in radius. Computation of nonlinear terms in spectral space is expensive, so nonlinear products and the Coriolis term are computed in physical space and then projected to spectral space at every time step. A standard 3/2-dealiasing in θ and φ is used at this stage. A hybrid of a Crank-Nicolson scheme for the diffusion terms and a second order Adams-Bashforth scheme for the nonlinear terms is used for integration in time.

A range of numerical resolutions has been used in this study varying from ($N_r = 61$, $N_l = 96$) in less demanding cases to ($N_r = 121$, $N_l = 144$) in more strongly stratified or turbulent runs. Correspondingly, the physical gridpoints on which non-linear terms are evaluated have been varied up to $N_r = 121$, $N_\theta = 216$, $N_\varphi = 437$.

2.4. Diagnostic output quantities

Our numerical convection and dynamo solutions are characterized by their kinetic and magnetic energy and heat transport given by a Nusselt number. The energies can be conveniently split into mean and fluctuating components, into poloidal and toroidal components and fur-

	Benchmark 1: Hydrodyn. convection	*Benchmark 2:* Steady dynamo	*Benchmark 3:* Unsteady dynamo
η	0.35	0.35	0.35
n	2	2	2
N_ρ	5	3	3
P	1	1	2
P_m	1	50	2
τ	2000	1000	40000
R	351806	80000	2.5e7
N_r / N_r	129 / 129	129 / 129	111 / 111
N_l / N_θ	128 / 128	128 / 128	120 / 144
N_m / N_φ	129 / 257	129 / 257	121 / 145
Timestep	4e-6	1e-6	1e-7
E	81.87991	4.19405e5	2.32730e5
$\overline{E}_p$	0.02201	53.0100	100.40
$\overline{E}_t$	9.37598	6.01725e4	1.81399e4
M	–	3.20172e5	2.58012e5
$\overline{M}_p$	–	1.69650e4	2.91155e4
$\overline{M}_t$	–	2.41185e5	1.17292e4
Luminosity	4.19886	11.50302	42.50992

Table 1: Comparison with the benchmark solutions proposed in [8].

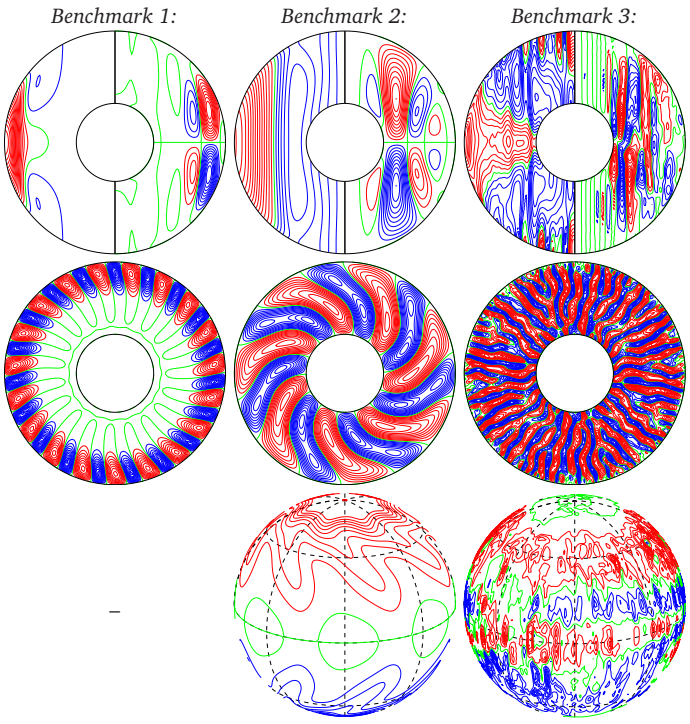

Figure 1: Solutions structures of benchmark cases 1, 2 and 3 (left to right). The first plot in each column shows azimuthally-averaged isocontours of $\overline{u}_\varphi$ (left half) and of the streamlines $r\sin\theta(\partial_\theta\overline{v})$ (right half) in the meridional plane. The second plot in each column shows isocontours of u_r in the equatorial plane. The third plot in each column shows isocontours of B_r at $r = r_o$.

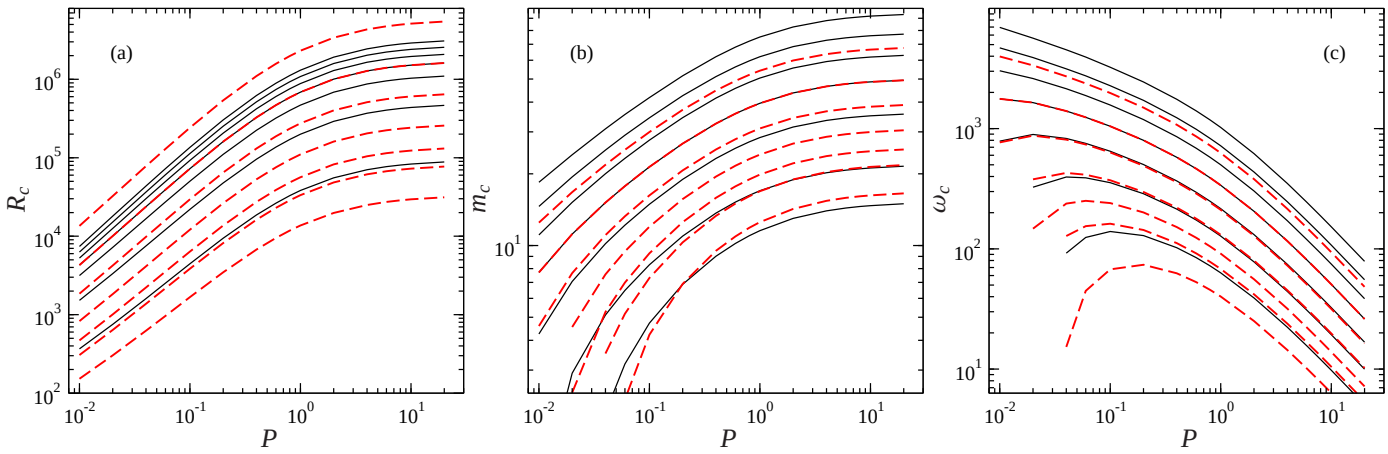

Figure 2: (a) The critical Rayleigh number R_c, (b) the critical wave number $m_{\rm crit}$ and (c) the critical frequency for onset of convection as functions of the Prandtl number P for $\eta = 0.65$, $\tau = 100, 200, 300, 500, 1000, 2000, 3000$, $n = 2$, (red dashed lines) and $N_\rho = 0.1, 1, 2, 3, 4, 5, 6$ (black solid lines) both increasing from bottom to top. The values are calculated using the quasi-geostrophic approximation of Busse and Simitev (2013).

ther into equatorially-symmetric and -antisymmetric components, thus giving a rather complete description of the scales of the convective flow and the multipole structure of dynamos. The mean and fluctuating toroidal and poloidal components of the kinetic energy are defined as

$$\bar{E}_p = \langle (\nabla \times (\nabla \bar{v} \times \boldsymbol{r}))^2/(2\bar{\rho})\rangle, \quad \bar{E}_t = \langle (\nabla r \bar{w} \times \boldsymbol{r})^2/(2\bar{\rho})\rangle, \quad (14a)$$

$$\check{E}_p = \langle (\nabla \times (\nabla \check{v} \times \boldsymbol{r}))^2/(2\bar{\rho})\rangle, \quad \check{E}_t = \langle (\nabla r \check{w} \times \boldsymbol{r})^2/(2\bar{\rho})\rangle, \quad (14b)$$

where angular brackets $\langle\rangle$ denote averages over the spherical volume of the shell. Magnetic energy components are defined analogously with h and g replacing v and w and without the factor $\bar{\rho}^{-1}$ within the angular brackets. The total energies are, of course, the sum of all components. The Nusselt number is defined as the ratio between the values of the luminosity of the convective state and of the basic conduction state,

$$Nu = -\frac{\exp(N_\rho)-1}{4\pi n c_1 \bar{\rho}(r_i)^n} \int_{\partial V} \kappa \bar{\rho}\bar{T}(\partial_r S)\boldsymbol{r}^2 \sin\theta d\theta d\varphi,$$

with the integral taken over the top surface ∂V. Apart from quantifying the heat transport of convection, the value of the Nusselt serves as a convenient proxy for the supercriticallity of the solution.

Other diagnostic quantities that are sometimes used to quantify convective and dynamo solutions can be derived from these quantities. For example, a non-dimensional magnetic Reynolds number, Rossby number and Lorentz number are given by

$$Rm = \mathrm{Pm}\sqrt{2E_{\rm kin}}, \quad Ro = \frac{2}{\tau}\sqrt{2E_{\rm kin}}, \quad Lo = \frac{2}{\tau}\sqrt{2E_{\rm mag}},$$

respectively.

3. Benchmarking and validation

To perform the numerical simulations of this study, we have extended our mature Boussinesq code [14, 2, 10, 3, 4, 11, 12] to solve the anelastic problem described in section 2. Despite similarities with the Boussinesq code, this is a major modification both in terms of the mathematical model and the numerical code. In order to validate the new code, we wish to report here a comparison with the anelastic dynamo benchmarks recently published by [8]. To aid comparison with the latter paper in this section only we employ the alternative nondimensionalisation used in [8] where the magnetic diffusion timescale rather that the viscous diffusion scale is adopted. Our output results from the three benchmark cases defined in [8] are summarized in table 1, and selected components of the solution are plotted in figure 1. We achieve near exact agreement with the results reported in [8] for the hydrodynamic case and the steady dynamo case, labeled *Benchmark 1* and *Benchmark 2* in table 1. Our results for the unsteady dynamo case labeled *Benchmark 3* in table 1 show certain insignificant differences from the values reported in [8]. The mean zonal flow we obtain in this case is 33% larger than that reported in the benchmark paper even though the angular momentum of our run remains smaller than 10^{-3}. This somewhat larger differential rotation gives rise to a magnetic field with energy 6% larger than that reported in the benchmark paper. The reasons for the discrepancy are that in this case we have imposed a two-fold azimuthal symmetry and used markedly lower resolution that the codes participating in [8]. This has been done to reduce computing time in this challenging case.

4. Similarities of anelastic and Boussinesq spherical convection and dynamos

Some linear results

These results are not intended to be comprehensive. Since the anelastic and the Boussinesq models are essentially different it is no obvious how to compare results directly. We will introduce a "supercriticallity" criterion – two cases with the same values of all basic parameters (4)

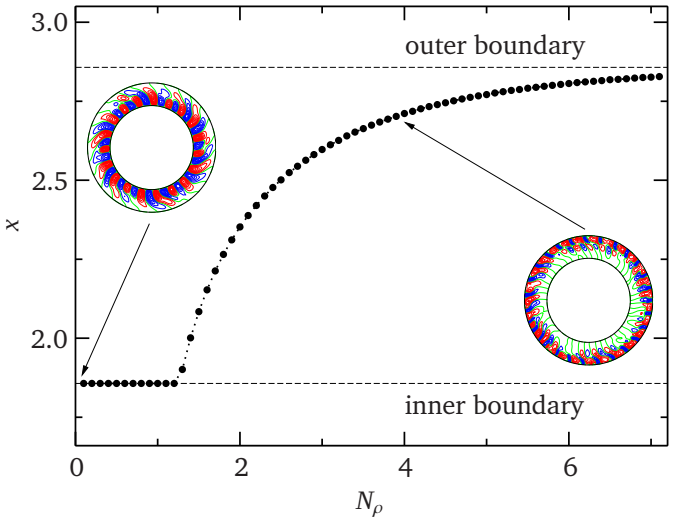

Figure 3:

apart from the Rayleigh number R are directly comparable if they have equal values of the ratio R/R_c, where R_c is the corresponding critical Rayleigh number for the onset of convection.

For this purpose, here we present R_c curves of typical cases we explore.

The main difference with Boussinesq convection is that onset of convection moves closer to the outer boundary - make new plot of position. Illustrate with case:

a.mv.e065p1t2r2500000m1p4N4.

Relaxation oscillations in anelastic convection

It is interesting that relaxation oscillations that have been found in Boussinesq simulations also appear in anelastic convection as seen in figures 4 and 5 for the case

ae035p1t40r20000000m4n2N3.

Another, case is

ae035p1t40r15000000m4n2N3.

In the presence of magnetic field relaxation oscillations disappear. However, the dynamic balance between diff rotation and magnetic fields produces oscillating dynamos. Here is a typical oscillation hemispherical dynamo, as shown in figures 6 and 7

(ae035p1t40r10000000m4p2n2N3).

This case is also interesting because the mean poloidal magnetic energy is dominant (both dipole and quadrupole) so it is a MD dynamo but the dynamo is oscillating as if it was and FD dynamo. The oscillations of the magnetic field are very regular with similar period twice as large as the period of the relaxation oscillations that have died out.

Increasing Rayleigh number we get slightly more dipolar oscillations as in the case

(ae035p1t40r15000000m4p2n2N3).

This case is not plotted as it is not significantly different from the previous case shown in 6 and 7.

Increasing both the Rayleigh number and the magnetic Prandtl number leads to much more dipolar oscillating case with APERIODIC reversals

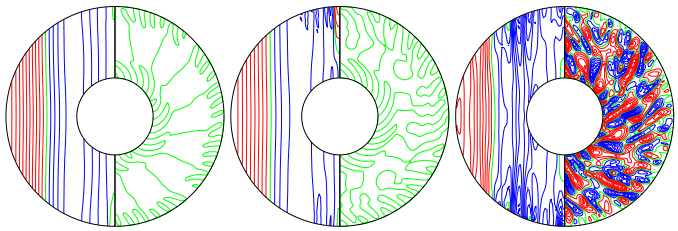

Figure 4: (ae035p1t40r20000000m4n2N3) A period of relaxation oscillations of convection in the case $\eta = 0.35$, $P = 1$, $\tau = 4 \times 10^4$, $R = 2 \times 10^7$, $n = 2$, $N_\rho = 3$, and four-fold azimuthal symmetry. The left halves of each plot show lines of constant $\overline{u}_\varphi$ in a meridional cut and the right halves streamlines, $r\partial_\varphi v$ = constant, in the equatorial plane. The separation in time is 0.02.

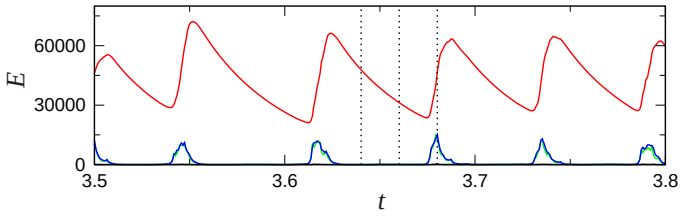

Figure 5: (ae035p1t40r20000000m4n2N3) Time series of energy densities of convection in the case plotted in 4. Red, blue and green lines indicate $\overline{E}_t$, $\overline{E}_t$, $\overline{E}_p$, respectively. $\overline{E}_p$ smaller by more than an order of magnitude than the other energy densities and has not been plotted for this reason. The three dotted vertical lines indicate the time instances where the snapshots in figure 4 are taken.

(ae035p1t40r15000000m4p4n2N3)

as shown in figures 8 and 9. Aperiodic reversals are interesting as a model of the geodynamo polarity reversals.

Dipolar Oscillations and benchmarks

The benchmark case is oscillatory and shows nice dipolar oscillations as illustrated in figure 10

(ben3.ae035p2t40r25000000m2p2n2N3)

Dipolar oscillations in thin shells

a.mv.e065p1t2r1200000m1p5N2 – Plot a sequence near t=85.

Magnetic field produces Solar-like differential rotation

A sufficiently strong magnetic field may counterbalance the geostrophic constraint and produce conical profile of the differential rotation with contours that are aligned in radial direction as shown in figure 11. This is reminiscent of the profile of the Solar differential rotation measured by helioseismology e.g. [9].

Comment that this is why Brandenburg and Jorg observe solar like diff rot in their coronal mass ejections - Jorg's thesis. http://arxiv.org/pdf/1301.2248.pdf

Banded differential rotation like Jupiter

See figure 12.

-ae035p1t40r10000000m4p2n2N3/um.59.pdf

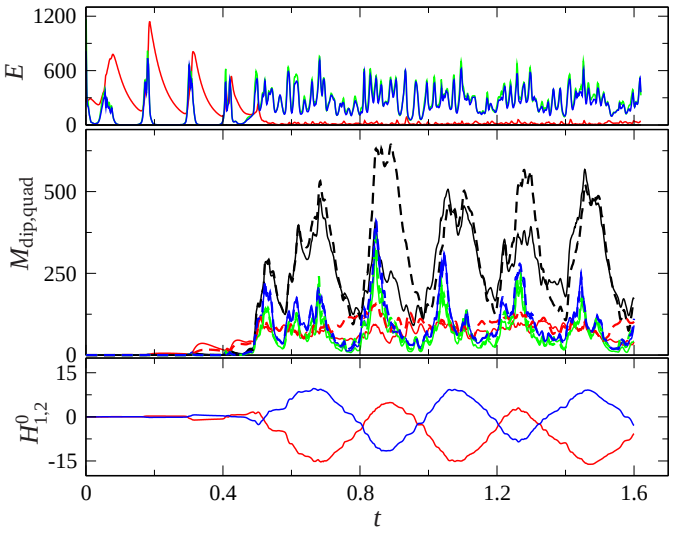

Figure 6: (ae035p1t40r10000000m4p2n2N3) Time series of energy densities of a hemispherical dynamo in the case $\eta = 0.35$, $P = 1$, $\tau = 4 \times 10^4$, $R = 10^7$, $P_m = 2$, $n = 2$, $N_\rho = 3$, and four-fold azimuthal symmetry. The upper panel shows kinetic energy densities of the velocity field. The second panel shows energy densities of dipolar components (thin solid lines) and quadrupolar components (thick brocken lines) of the magnetic field. The mean toroidal components are represented by red lines, the fluctuating toroidal – by blue lines, the mean poloidal – by black lines and the fluctuating poloidal – by green lines. The lowest panel shows the coefficient of the axial dipole component H_1^0 (red line) and the coefficient of the axial quadrupole component (blue line) at $r = r_i + 0.5$.

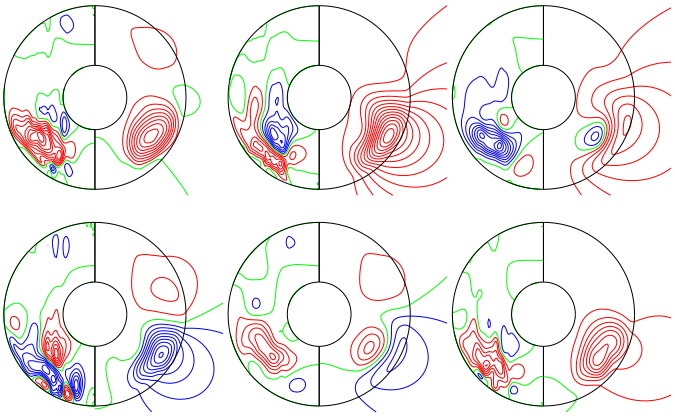

Figure 7: (ae035p1t40r10000000m4p2n2N3) A period of hemispherical dynamo oscillations in the case shown in figure 6. The left half of each plot shows lines of constant $\overline{B}_\varphi$ and the right half shows meridional field lines $r \sin\theta \partial_\theta \overline{h}$ = const. Plots are arranged row-by-row and the separation in time is 0.08.

-Magnetic field is important - see the effect of hemispherical dynamo - this case is good to use as figs of magn field already included 6 & 7. — Perhaps no evidence for this.

At stronger magnetic fields band structure does not persist and radially-constant conical Solar profiles of diff rot emerge as in figure 10.

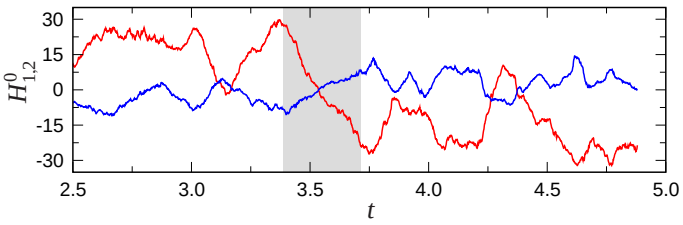

Figure 8: (ae035p1t40r15000000m4p4n2N3) Aperiodicaly reversing dynamo. Shown are time series of coefficient of the axial dipole component H_1^0 (red line) and the coefficient of the axial quadrupole component (blue line) at $r = r_i + 0.5$ in the case $\eta = 0.35$, $P = 1$, $\tau = 4 \times 10^4$, $R = 1.5 \times 10^7$, $P_m = 4$, $n = 2$, $N_\rho = 3$, and four-fold azimuthal symmetry. One reversal happens within the shaded area when the dipole component changes sign.

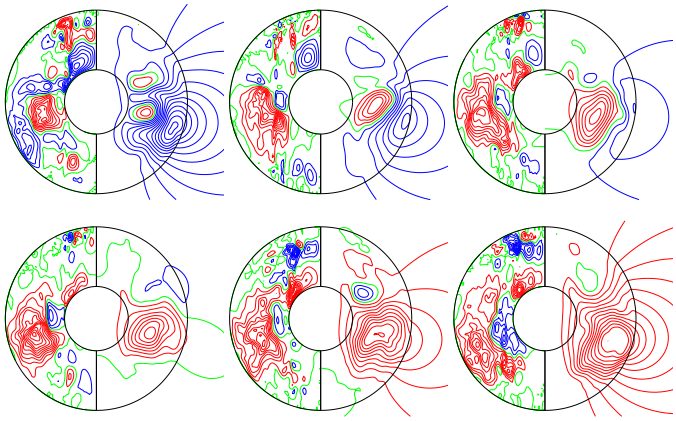

Figure 9: (ae035p1t40r15000000m4p4n2N3) An apperiodic reversal of the dynamo shown in figure 8. The left half of each plot shows lines of constant $\overline{B}_\varphi$ and the right half shows meridional field lines $r \sin\theta \partial_\theta \overline{h}$ = const. Plots are arranged row-by-row and the separation in time is 0.04 falling in the shaded area of figure 8.

Subsurface decrease of differential rotation

This is very interesting, see cases
a.e065p1t2r2000000m1p6N3.mv.vc (time 18 to 20)
and
(a.e065p1t2r1800000m1p8N3.mv.vc) and
(a.e065p1t2r1800000m1p8N3.mv.vc.per).
— Do these oscillate?
— Can we find equatorward propagation?
Oscillating cases:
a.mv.e065p1t2r2000000m1p4N3
a.e065p1t2r2000000m1p6N3.mv.vc
a.mv.e065p1t2r2000000m1p6N3
a.mv.e065p1t2r2000000m1p4N3-sequence
a.mv.e065p1t2r2500000m1p4N3

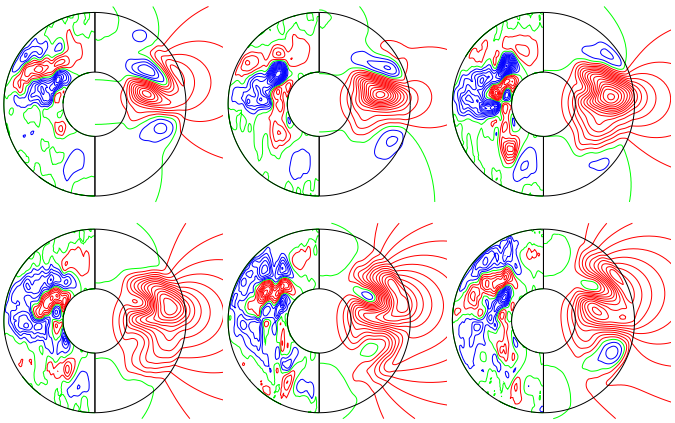

Figure 10: (ben3.ae035p2t40r25000000m2p2n2N3) A period of dipolar dynamo oscillations in the benchmark case $\eta = 0.35$, $P = 2$, $\tau = 4 \times 10^4$, $R = 2.5 \times 10^7$, $P_m = 2$, $n = 2$, $N_\rho = 3$, and two-fold azimuthal symmetry. The left half of each plot shows lines of constant $\overline{B}_\varphi$ and the right half shows meridional field lines $r \sin\theta \partial_\theta \overline{h} = \text{const}$. Plots are arranged row-by-row and the separation in time is 0.015.

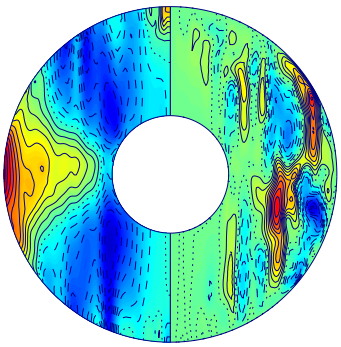

Figure 11: (ben3.ae035p2t40r25000000m2p2n2N3) Solar-like differential rotation $\overline{u}_\varphi = \text{const}$. in the left halves of the plot and azymuthally-averaged meridional circulation in the right halves in the case shown in figure 10. The plots are time averaged over a period of 0.005.

High Prandtl number convection looks very solar like

a.e075p5t05r800000m1N3.sf.vc.Di0.plt.22.pdf

Note the double-cell meridional circulation and the tendency towards conical profiles of diff rotation.

Variable viscosity

Thin downwelling and thick upwelling
a.e065p04t04r300000m1p2.sf.vr4
a.e065p06t06r600000m1p2.sf.vr4.plt.11.pdf
Compare cases with otherwise fixed parameters:
a.e075p5t05r800000m1N3.sf.vr.plt.28.pdf
a.e075p5t05r800000m1N3.sf.vc.plt.16.pdf
Cases with fixed params:
a.e065p05t03r300000m1N3.sf.vc,
a.e065p05t03r300000m1N3.sf.vr,
a.e065p05t03r300000m1N3.sf.vrkr
a.e065p1t1r800000m1N3.sf.vc,
a.e065p1t1r800000m1N3.sf.vr,
a.e065p1t1r800000m1N3.sf.vrkr

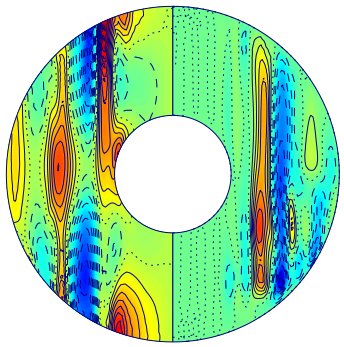

Figure 12: (ae035p2t40r15000000m4p2n2Nrho3a) Jupiter-like banded differential rotation $\overline{u}_\varphi = \text{const}$. in the left halves of the plot and azymuthally-averaged meridional circulation in the right halves in the case $\eta = 0.35$, $P = 2$, $\tau = 4 \times 10^4$, $R = 1.5 \times 10^7$, $P_m = 2$, $n = 2$, $N_\rho = 3$, and four-fold azimuthal symmetry.

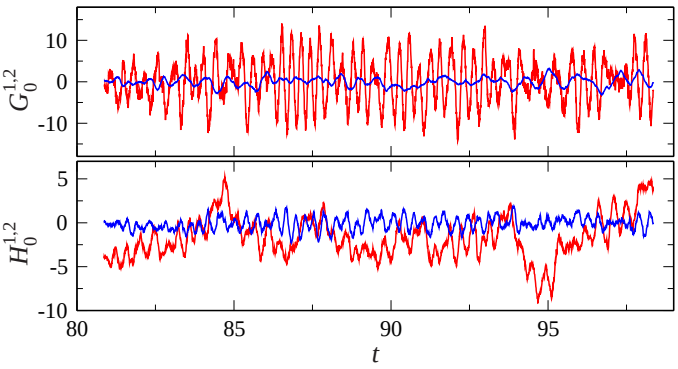

Figure 14: (a.mv.e065p1t2r2500000m1p4N3) Dipolar oscillations shown in the timeseries of the the axisymmetric toroidal coefficients G_0^1 (red) and G_0^2 (blue) and the axisymmetric poloidal coefficients H_0^1 (red) and H_0^2 (blue) describing the main dipolar and poloidal contributions in the spherical harmonics expansion of the magnetic field in the case $\eta = 0.65$, $P = 1$, $\tau = 2 \times 10^3$, $R = 2.5 \times 10^6$, $P_m = 4$, $n = 2$, $N_\rho = 3$ shown in figure 13.

5. Buoyancy-dominated convection

Discussion of case (a.e065p1t2r10000000m1p2N3n2.sf.vc) shown in figures 17 and 18. The influence of the magnetic field is quite remarkable. Consider the following observations illustrated in figures 17 and 18:

- pure convection - diff rot is monotonously increasing/decreasing towards the outer surface in the prograde/retrograde case.
- pure convection in the buoyancy-dominated regime is retrograde.
- pure convection - does not show columnar structure at depth.
- dynamo - the energy of the self-sustained magnetic field is an order of magnitude smaller that the kinetic energy.

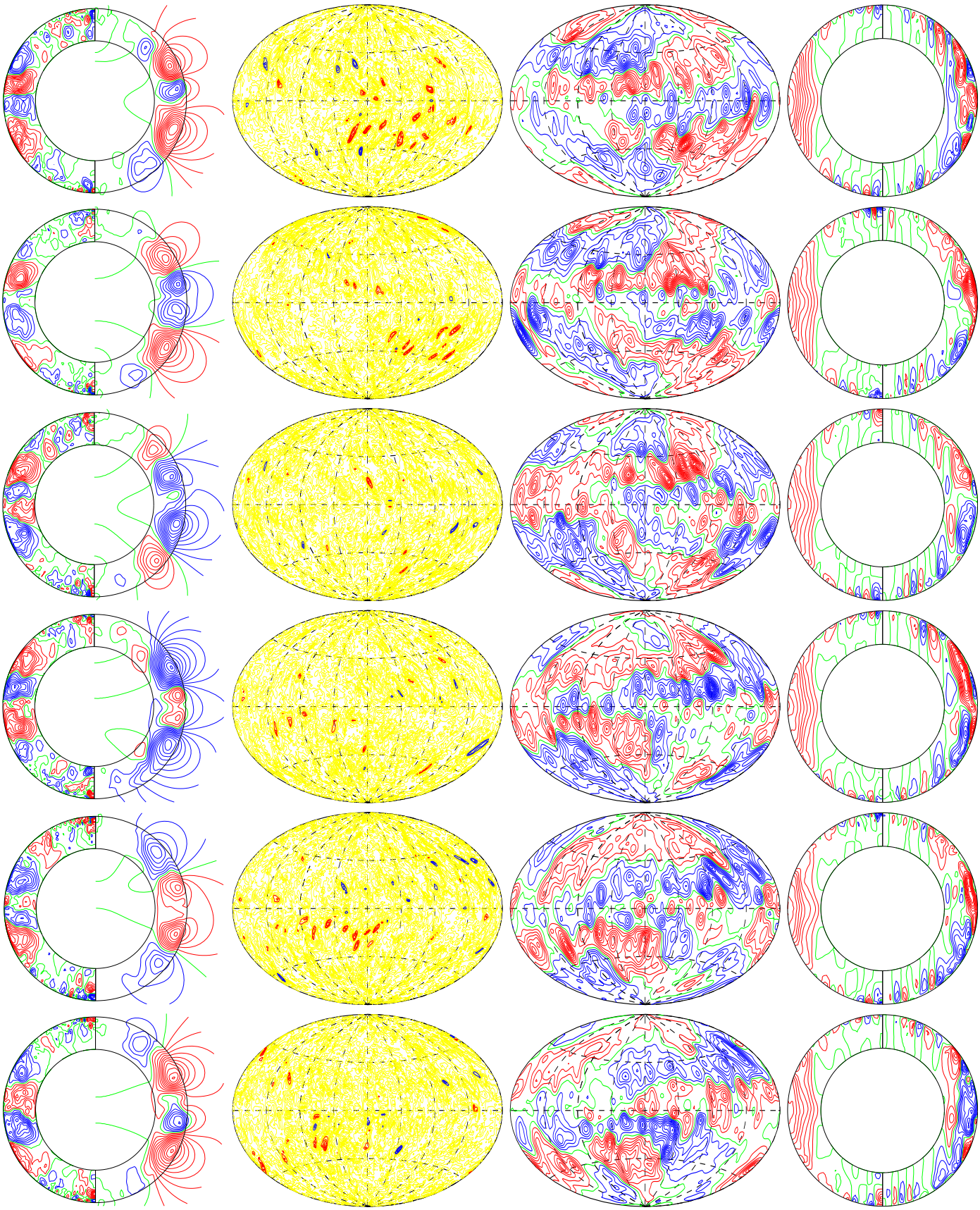

Figure 13: (a.mv.e065p1t2r2500000m1p4N3) One period of dipolar oscillations.

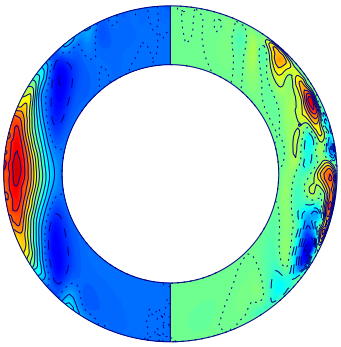

Figure 15: (a.e065p1t2r1800000m1p8N3.mv.vc) Solar like (sub-surface decrease) differential rotation $\overline{u}_\varphi$ = const. in the left halves of the plot and azymuthally-averaged meridional circulation in the right halves in the case $\eta = 0.65$, $P = 1$, $\tau = 2 \times 10^3$, $R = 1.8 \times 10^6$, $P_m = 8$, $n = 2$, $N_\rho = 3$.

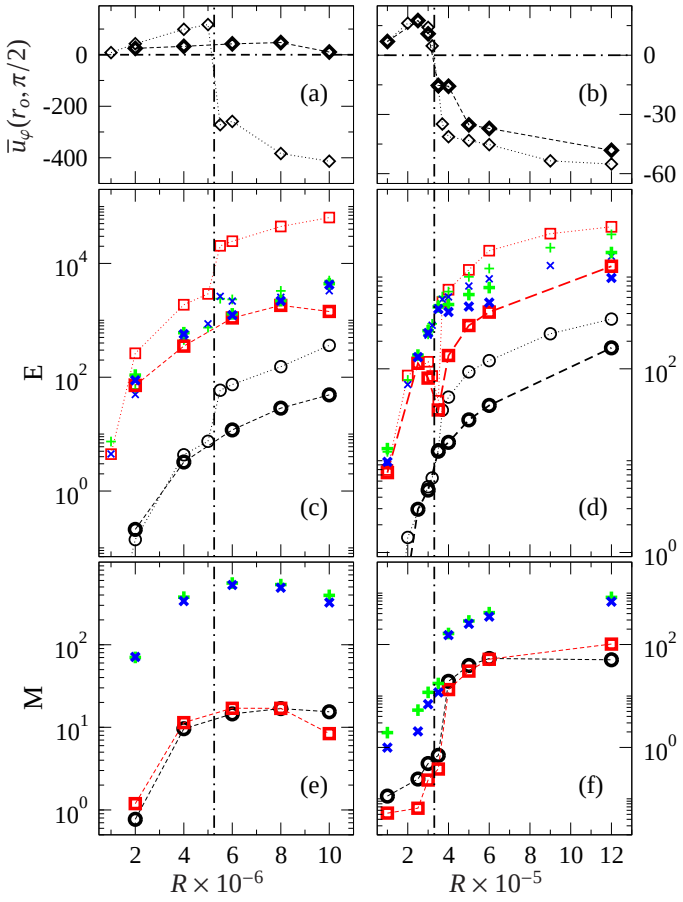

Figure 16: (a,b) Equatorial zonal flow at the equator $\overline{u}_\varphi(r_o, \pi/2)$. (c,d) Average kinetic energy densities and (e,f) average magnetic energy densities as functions of the Rayleigh number R in the cases (a,c,e) $\eta = 0.65$, $P = 1$, $\tau = 2000$, $n = 2$, $N_\rho = 3$, and (b,d,f), $\eta = 0.65$, $P = 0.5$, $\tau = 300$, $n = 2$, $N_\rho = 3$ Nonmagnetic convection cases are denoted by thin symbols in (a,b,c,d). Dynamo cases are denoted by thick symbols in all panels and have $P_m = 2$ in (a,c,e) and $P_m = 6$ in (b,d,f). Black circles, red squares, green pluses and blue crosses denote $\overline{X}_p$, $\overline{X}_t$, $\tilde{X}_p$, $\tilde{X}_t$, with $X = E, M$. Vertical dash-dotted lines denote the transition to buoyancy-dominated regime.

- dynamo - diff rotation is reversed from retrograde to prograde by even by such relatively weak magnetic field.
- dynamo - differential rotation has a maximum inside the shell and then shows a subsurface decrease.
- dynamo - convective columns are visible in depth.
- dynamo - has a strong dipolar symmetry because of the strong polar convection. Unfortunately this dipole does not oscillate.

Question - Is there a transition from multipolar to dipolar dynamos with the increase of R? There must be - in the prograde regime at low R thin shell dynamos are mixed multipolar; in the retrograde regime at high R dipolar dynamos are found as figure 18 demonstrates. There must be a transition in between - look at newly started sequences.

5.1. *Interesting Boussinesq cases*

a.mv.e065p1.2t2r500000m1p4.5N001 - maybe we should start cases with slowly increasing N_ρ to follow transitions. What will quadrupolar dynamos become?

Effects of radial variations of viscosity and diffusivity

Evidence of localized convection or spotty convection

- I have also thinking about your paper. It could be interesting to plot wavenumber m (number of equatorial cells) as function of tau and Pr, 0.1iPri2 for convenient value of r and N3 because there is this remarkable transition from low m to high m as function of mainly Pr. I am wondering whether this transition may be hysteretic. Yours,F.

  Thank you for the suggestion. Few questions, that will help a lot: - Why do you think this is remarkablle? In Boussinesq linear analysis it is not uncommon to see a jump in wavenumber, even a large jumps say fig 1 from our paper in GAFD-2005.

  Here we have a much more dramatic phenomenon. I GAFD m changed from 2 at Pr=0.2 to 3 for Pr=2 and similar changes with higher m at at higher tau. In the a-case it changes from m=7 at Pr=0.3 to m=20 at Pr=1.

  - How will we select comparable cases when we vary Pr? Clearly this will be only a rough comparison, but we need to achive approx the same supercriticallity as Pr is varied. This question is actually worrying me.

  At fixed t the critical R should not vary that much. It seems to me that there could be substantial hysteresis.

  It would be nice to have a liner code so we can find critical R.

  Apparently Wicht used one supplied by Chris Jones. It will be important to use a case of nu(r) which has a reasonable deviation of s from the S-reference

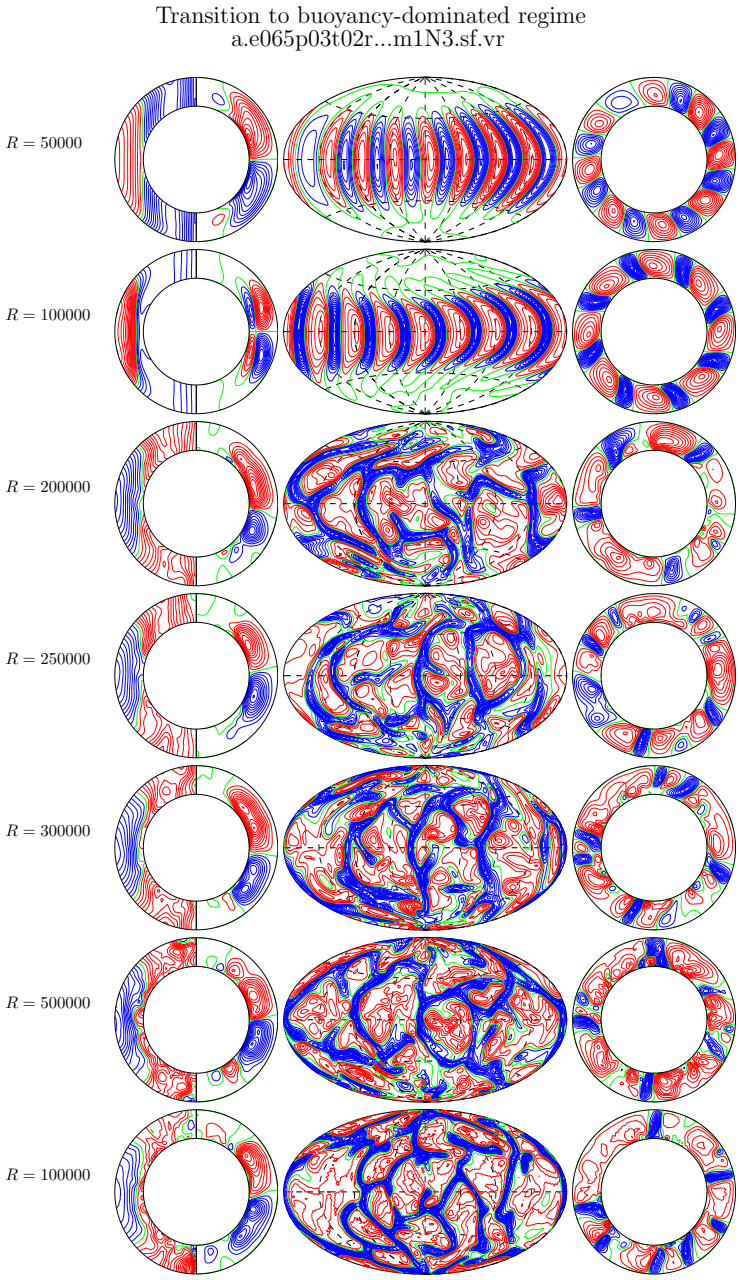

Figure 19: A figure like this but from the sequences in figure 16.

throughout the layer such the influence of convection filling only part of the layer is minimized.

- Neat separation between convection in the tangent cylinder and convection in the polar regions
- Asymmetry of descending and ascending flows - this is visible in most cases at small Pr and τ. - include a characteristic plot, say,

  a.e065p05t03r300000m1N3.sf.vr

  and similar.
- Transition to retrograde differential rotation. - Many cases, most accessible for low values of τ. Can we reach beyond this regime? What are dynamos like in the regime of retrograde diff rotation. In this regime diff rotation is substantially decreasing towards the surface, so according to Yoshimura dynamo waves should travel towards the equator.
- Spread of convection throughout the layer - in models with variable viscosity (when $\nu = \bar{\rho}^{-1}$ is constant DYNAMIC viscosity).
- In models with variable viscosity (when $\nu = \bar{\rho}^{-1}$ is constant DYNAMIC viscosity) convection spreads throughout the layer and not only near the surface as in the simulations of Whicht and of Jones. So each time

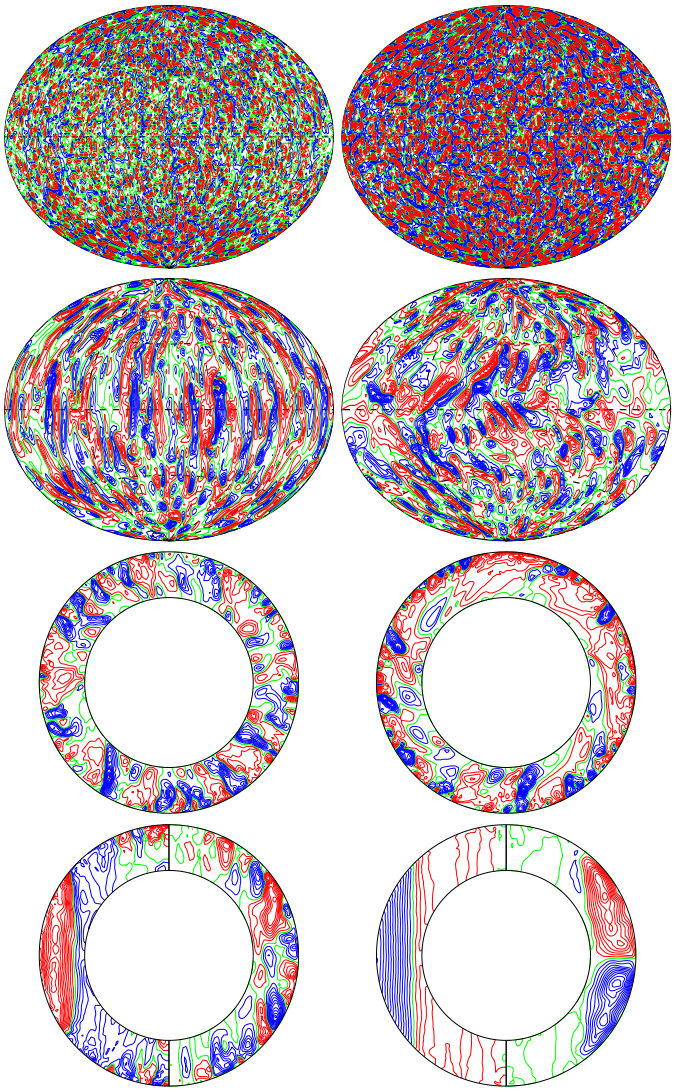

Figure 17: (a.e065p1t2r10000000m1p2N3n2.sf.vc and a.e065p1t2r10000000m1N3n2.sf.vc) Left column: dynamo case a.e065p1t2r10000000m1p2N3n2.sf.vc; Right column: convection only case a.e065p1t2r10000000m1N3n2.sf.vc. Row one: u_r at $r = 0.95 + r_i$; Row two: u_r at $r = 0.3 + r_i$; Row 3: pol streamlines in the equatorial plane; Row 4: $\overline{u}_\varphi$ and mer streamlines average over a period of 0.025.

when they claim that a particular mechanism is due to this effect they may not be right.

- Double-cell meridional circulation as per Junwei Zhao, poleward flow near surface.

6. Conclusion

Summary of results.

- We have shown that even a rather small increase of the value of the Prandtl number above unity can produce profiles of the differential rotation that deviate significantly from geostrophy even in rather laminar solutions. When such differential rotation profiles

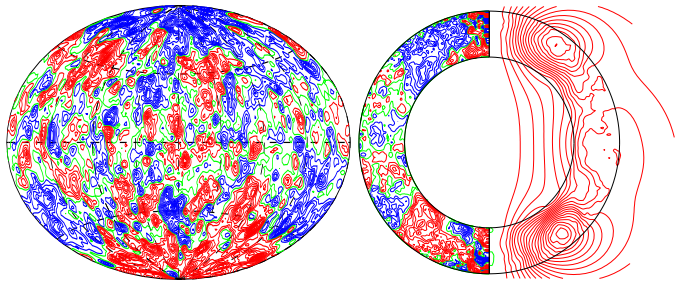

Figure 18: (a.e065p1t2r10000000m1p2N3n2.sf.vc) Magnetic components of the same case as in the left column of figure 17. Left plot: B_r at $r = 1.13 + r_i$; Right plot:: $\overline{B}_\varphi$ and mer fieldlines average over a period of 0.025.

are further affected by self-sustained magnetic field differential rotation not unlike the one inferred from helioseismological observations can be found.

Discussion and implications.

- The results may be relevant as a model of Solar magnetic field oscillations, structure of the Solar convection zone, and differential rotation.
  - **Solar cycle –** The direction of dynamo waves in self-consistent simulations with prograde differential rotation is always from equator to poles in contrast to observations. We wish to check whether retrograde differential rotation generated in the buoyancy-dominated regime may reverse the direction of dynamo waves so that they propagate from poles to equator in agreement with observations.
  - **Structure of convection zone –** It will be of interest to find whether different regimes of convection may develop in the inner and at the outer part of the shell simultaneously so that organised geostrophic convection is hidden below a near-surface layer of well-mixed ("turbulent") convection. We believe that such a configuration is similar to the structure of the Solar convection zone. Indeed, it is well established by observation of the surface velocities and magnetic fields that buoyancy effects dominate near the surface. As a result the near-surface flows and magnetic fields are strongly turbulent and lack any global organization. On the other hand, the regularity of the 11-year Solar cycle is also well established and the regular reversals cannot be achieved without large-scale organized field and flow. We would like to argue that the organized columnar structures that are characteristic in the rotation-dominated regime will play this role.

    Variation in density is a necessary ingredient in this scenario. Indeed, in the Boussinesq approximation, the rotation parameter τ and the

critical Rayleigh number R_c are constant throughout the shell. This means that the entire volume of the shell will be either in the rotation-dominated or the buoyancy-dominated regime. In contrast, the anelastic approximation allows for radial variation in density, viscosity and entropy diffusivity so that τ and R_c vary with radius. In this way, one may hope to achieve a configuration where the inner part of the shell is in the rotation-dominated regime and the outer part is in the buoyancy-dominated regime.

  - **Solar differential rotation –** Finally, differential rotation may also assume more Solar-like profile.

- In fact, variation in density only may not be sufficient to produce Solar-like differential rotation as indicated by Gastine et al. In this case convection flows in the rotation-dominated region are relatively weaker by comparison with flows in the buoyancy-dominated near-surface layer. A stronger organized flow is likely needed to produce the solar-lice cyclic oscillations and differential rotation profile.

Future directions. – Include radial variation of viscosity and entropy diffusivity.

– Go beyond the buoyancy-dominated regime into regime III.

– Explore parameter regime so as to find periodic reversals. Will they propagate equator-wise?

Acknowledgment

This research has been supported by NASA Grant NNX-09AJ85G. RDS and FHB acknowledge the hospitality of Stanford University and UCLA. RDS enjoyed a period of study leave granted by the University of Glasgow.

References

[1] J. Aurnou, M. Heimpel, and J. Wicht. The effects of vigorous mixing in a convective model of zonal flow on the ice giants. Icarus, 190(1):110–126, 2007.

[2] F. H. Busse, E. Grote, and R. D. Simitev. Convection in rotating spherical shells and its dynamo action. In Jones C.A., Soward A.M., and Zhang K., editors, Fluid Mech. Astrophys. Geophys. Series vol. 11: "Earth's Core and Lower Mantle", pages 130–152. Taylor and Francis, London,, 2003.

[3] F. H. Busse and R. Simitev. Parameter dependences of convection-driven dynamos in rotating spherical fluid shells. Geophys. Astrophys. Fluid Dyn., 100:341, 2006.

[4] F. H. Busse and R. Simitev. Toroidal flux oscillations as possible causes of geomagnetic excursions and reversals. Phys. Earth Planet. Inter., 168:237, 2008.

[5] T. Gastine, J. Wicht, and J. Aurnou. Zonal flow regimes in rotating anelastic spherical shells: an application to giant planets. 225:156–172, 2013.

[6] P. A. Gilman. Theory of convection in a deep rotating spherical shell, and its application to the sun. In V. Bumba and J. Kleczek, editors, "Basic Mechanisms of Solar Activity", Procs. IAU Symposium 71, page 207. D. Reidel Pub. Co., Boston, 1976.

[7] D. O. Gough. The anelastic approximation for thermal convection. J. Atmos. Sci., 26:448, 1969.

[8] C. A. Jones, P. Boronski, A. S. Brun, G. A. Glatzmaier, T. Gastine, M. S. Miesch, and J. Wicht. Anelastic convection-driven dynamo benchmarks. Icarus, 216(1):120–135, 2011.

[9] J. Schou et al. Helioseismic studies of differential rotation in the solar envelope by the solar oscillations investigation using the michelson doppler imager. Astrophys. J., 505:390, 1998.

[10] R. Simitev and F. H. Busse. Prandtl-number dependence of convection-driven dynamos in rotating spherical fluid shells. J. Fluid Mech., 532:365, 2005.

[11] R. Simitev and F. H. Busse. Bistability and hysteresis of dipolar dynamos generated by turbulent convection in rotating spherical shells. EPL, 85:19001, 2009.

[12] R. Simitev and F. H. Busse. How far can minimal models explain the solar cycle? Astrophys. J., 749:9, 2012.

[13] A. Tilgner. Spectral methods for the simulation of incompressible flows in spherical shells. Int. J. Numer. Meth. Fluids, 30(6):713–724, 1999.

[14] A. Tilgner and F.H. Busse. Finite-amplitude convection in rotating spherical fluid shells. J. Fluid Mech., 332:359–376, 1997.